The Influence of Preset Pitch on the Performance of Cambered Foils within Cross-flow Turbines

Han-Wen Chi

A thesis
submitted in partial fulfillment of the
requirements for the degree of

Master of Science

University of Washington

2024

Committee:

Owen Williams

James Hermanson

Program Authorized to Offer Degree:
Department of Aeronautics and Astronautics

University of Washington

Abstract

The Influence of Preset Pitch on the Performance of Cambered Foils within Cross-flow Turbines

Han-Wen Chi

Chair of the Supervisory Committee:
Owen Williams
Department of Aeronautics and Astronautics

The rotational reference frame in cross-flow turbines results in variations in virtual geometry and the angle of attack as the blades move through the flow field. This dynamic interaction significantly affects the performance and efficiency of the turbine. Initial studies have looked at the influence of blade geometric camber, either enhancing or reducing the virtual camber due to rotation. Other studies have shown the importance of preset pitch for overall performance. In this study, the sensitivity of the flow curvature effects to the change in preset pitch angle and airfoil camber are examined, with the virtual camber and angle of attack estimated according to the conformal mapping method. The virtual camber and angle of attack caused by rotation are shown to be more sensitive to the preset pitch angle than to changes in geometric camber. The interaction of preset pitch angle and geometric camber across a range of tip-speed ratios was examined for a single-bladed turbine with both a symmetric foil and those with $\pm 2\%$ camber. It was found that the preset pitch (-6° to -8°) and tip-speed ratio (3.0) that yield optimal performance for each blade were insensitive to geometric camber. However, the utilization of the $+2\%$ camber airfoil does not significantly increase the peak performance of the turbine with any combination of the preset pitch angle tested. The positive preset pitch angle and the positive camber enhance the lift upstream and have a more detrimental performance downstream, while the negative preset pitch angle

and negative camber do the opposite. Often the preset pitch angle or the airfoil camber has the peak performance upstream and does not correspond to the optimal performance downstream. The turbine loading has a direct relationship to the blade power. Three camber foils yield similar average turbine loading around optimal performance and are insensitive to the preset pitch angle at a lower tip-speed ratio. The negative camber airfoil could reduce the maximum loading on the turbine by 16% with no loss in performance when compared to the zero camber airfoil.

TABLE OF CONTENTS

LIST OF FIGURES

NOMENCLATURE

α: Angle of attack

α_p: Preset pitch angle

α_r: Induced angle of attack due to rotation

C_P: Phase-averaged coefficient of power, $C_P = \frac{\omega\tau}{\frac{1}{2}\rho U_\infty^3 2RL}$

$\overline{C_P}$: Time-averaged coefficient of power

C_F: Phase-averaged coefficient of force, $C_F = \frac{F}{\frac{1}{2}\rho U_\infty^2 2RL}$

$\overline{C_F}$: Time-averaged coefficient of force

C_{Fmax}: Maximum phase-averaged coefficient of force

F_r: Froude Number

γ_g: Geometric camber

γ_r: Induced camber due to rotation

L: Turbine blade length (Turbine height)

λ: tip-speed ratio (TSR)

R: Turbine radius

Re: Reynolds number

Re_D: Reynolds number calculated from the diameter of the turbine

τ: Torque

U_∞: Free stream flow velocity

ω: Angular velocity

$\frac{c}{R}$: chord-to-radius ratio

ACKNOWLEDGMENTS

First of all, I would like to express my heartfelt gratitude to Prof. Owen Williams for his patience and guidance throughout the research process. This endeavor would not have been possible without his knowledge or expertise shared with me. In addition, He has been incredibly supportive and understanding, especially during times when I was overwhelmed with schoolwork, research, and family issues. Prof. Williams granted me the flexibility I needed in scheduling my work, which has been immensely helpful. It has been an enriching journey working with him for the past three years since my undergraduate studies.

I am also thankful to Ari Athair and Abigale Snortland, my fellow lab mates, for their technical support, guidance in the current project, and valuable feedback during our sessions. A special mention goes to Ari for his assistance during the two weeks of intense data collection. Their moral support has been a constant source of encouragement, and I am truly grateful for their presence throughout this endeavor.

Special thanks to my friends and family, especially my girlfriend Yutong Zhao, for their unwavering support, understanding, and care. Yutong's cooking and delivery during my all-nighters brought comfort and sustenance, supporting me through the most challenging phases of my project.

DEDICATION

To the 18 years I've spent pursuing academic endeavors.

Chapter 1
INTRODUCTION

One of the benefits of cross-flow turbines is the insensitivity to the inflow direction. It has been shown that cross-flow turbines, when deployed in an array formation, can improve the power production density under the same area when compared to conventional wind turbines [2]. On the other hand, the turbine blade experiences a large range of angles of attack (AOA) which causes complexity in analyzing flow behavior around the blade with the presence of unsteady flow, dynamic stall behavior, and dynamics of the forces acting on the blade. Such complexity increases the difficulty of turbine design and increases the complexity of characterizing the turbine performance. Due to the rotational reference frame, rotationally-induced changes to blade camber and angle of attack vary with blade position and the ratio of the blade chord and turbine radius, c/R, and can be as large as 15% or 18° at low rotation rates. While it is theoretically possible to calculate these geometric changes if turbine induction is neglected [3] the impact on performance is poorly understood. Recent work by Athair et al. [4] has highlighted that it is possible to increase performance by introducing a geometric camber in the direction that reduces performance in the upstream power stroke due to improvements in flow recovery in the downstream stroke. It is also known that the blade preset pitch value (its angle to the freestream when the blade is facing directly upstream) influences turbine performance for blades with zero camber [5, 6]. The connection between the preset pitch angle and the airfoil camber has not yet been investigated. A potential performance benefit from coupling the preset pitch angles and camber could exist. This work aims to explore the impact of the geometric camber, in combination with changing blade preset pitch angle, on the performance and loading of cross-flow turbines.

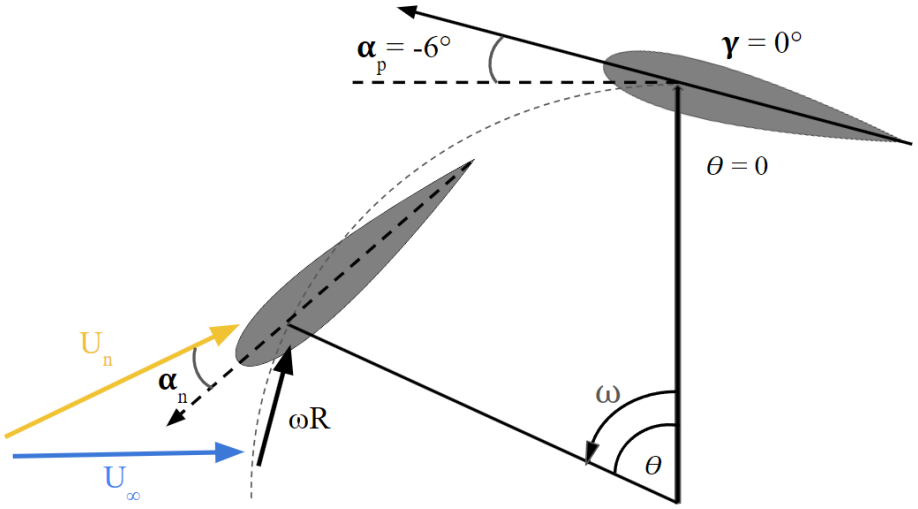

Figure 1.1: Turbine coordinate system.

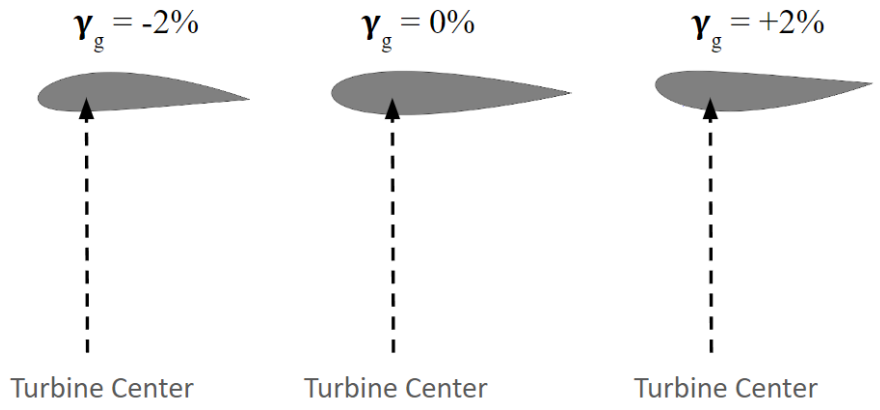

Figure 1.2: Camber direction.

We define the coordinate system for the cross-flow turbine as shown in Fig. 1.2. The turbine radius R is the distance from the center of the turbine to the outmost point of the blade. The relative angles and positions are defined through the quarter chord of the blade

at location $\frac{c}{4}$. The direction of the inflow U_∞ is shown as the blue arrow pointing to the right. The azimuthal location $\theta = 0$ is defined to be zero as the turbine blade points directly at the inflow direction. The turbine blade rotates in a counterclockwise direction, hence θ is positive in a counterclockwise direction. The preset pitch angle α_p is the angle between the blade chord line to the tangential line of the turbine rotation. The angle is defined to be negative when it is pitching outward from the center of the turbine, conversely, α_p is positive when it is pointing inward towards the center of the turbine. A preset pitch value of $-6°$ has been shown to be close to optimal across a range of turbines and operating conditions [5]. The camber direction is defined as Fig. 1.2, positive camber when curves away from the center of the turbine, and negative camber when curves toward the center of the turbine. Positive preset pitch angle and positive camber correspond to the direction where the upstream lift is enhanced.

Under constant-speed control, the key non-dimensional variable is the tip-speed ratio (TSR), defined as, $\lambda = \frac{\omega R}{U_\infty}$. It represents the relationship between the rotational velocity at the edge of the turbine and the inflow velocity. Under normal operations, for a set of operating conditions and turbine configurations, the turbine performance varies with the tip-speed ratio and there exists an optimal tip-speed ratio [5]. The nominal relative velocity U_n is the resultant vector from the summation of the inflow velocity vector U_∞ and the angular velocity vector ωR. This is the relative flow experienced by the blade calculated purely from the geometric parameters and neglecting turbine induction. The nominal velocity can be expressed in terms of tip-speed ratio λ and θ.

$$U_n(\theta) = \sqrt{\lambda(\theta)^2 + 2\lambda(\theta)\cos(\theta) + 1} \tag{1.1}$$

The nominal angle of attack is the angle between the blade chord line to the nominal velocity vector at each azimuthal location. The equation for the nominal angle is expressed as,

$$\alpha_n(\theta) = -\tan^{-1}\left(\frac{\sin(\theta)}{\lambda(\theta) + \cos(\theta)}\right) + \alpha_p \tag{1.2}$$

since the turbine blade endures dynamic events such as constantly changing inflow direction relative to the blade. This geometric approach to the nominal relative velocity and the

nominal angle of attack neglects the near-blade hydrodynamics or the induction, but the approximation provides us with some understanding of the flow behavior to the near-blade region geometrically.

Migliore et al. [1] present a mapping method to transform an airfoil in a rotational flow field to its equivalent cambered airfoil in a rectilinear flow field. The virtual geometry is dependent on local blade-relative velocity and angle of attack, which we take from the relations for the nominal conditions, given above. The magnitude of the virtual camber, γ_r, and angle of attack α_r is sensitive to the chosen tip-speed ratio and chord-to-radius ratio and varies throughout the turbine rotation. As a result, no fixed airfoil can fully cancel these virtual geometry changes due to rotation. In this study, the influence of geometric camber and preset pitch on the virtual geometry is also explored using the method of Migliore et al. [1]. The total angle of attack and camber are defined as the summation of nominal or geometric components, as

$$\alpha = \alpha_n + \alpha_r \qquad \gamma = \gamma_g + \gamma_r \tag{1.3}$$

Previous studies have explored the performance of turbines with $c/R = 0.47$ with the symmetric NACA0018 airfoil [7, 8, 6]. Athair et al. [4] examined the virtual component and analyzed the performance of cross-flow turbines under the NACA2418 airfoil. The NACA2418 airfoil with a 2% camber with its maximum camber at the 40% chord line counting from the leading edge was where the virtual calculation shows the maximum camber location. The resultant plots of virtual camber and virtual AOA were shown to be insensitive to the geometric camber with a 2% magnitude. This additional 2% camber can concave inward towards the rotation center or concave outward away from the rotation center. The concave inward case is defined to be the negative camber and the concave outward case is the positive camber case. Results have shown the camber which increases the performance in the upstream ($\theta = 0^\circ - 180^\circ$) is often offset by the detrimental performance in the downstream ($\theta = 180^\circ - 360^\circ$).

Strom et al. [6] and Hunt et al. [5] stated the influence of preset pitch angle is more significant when compared to other variables including aspect ratio, solidity, and chord-to-

radius ratio. Hunt et al. [5] tested the influence of a wide range of characteristic variables on turbine performance. These variables include the blade number N, the chord-to-radius ratio $\frac{c}{R}$, preset pitch angle α_p, and Reynolds number measured from the diameter of the turbine Re_D. Each variable was found to affect turbine performance differently and this study matches one of the Reynolds numbers used by Hunt et al. [5]. In general, a preset pitch of $\alpha_p = -6^\circ$ yields close to optimal performance with slight variations when changing the chord-to-radius ratio, tip-speed ratio, and Reynolds number.

This work aims to explore the effects of preset pitch angles in combination with geometric camber under a wide range of TSR. We analyzed the sensitivity of virtual geometry effects due to preset pitch angles and geometric camber through the mapping method of Migliore et al. [1]. Subsequently, we experimentally collected performance and force data for a single-blade turbine to show the phase-dependent variation through different turbine geometries. The objective is to provide insight into the effects of preset pitch angles on camber blades and to determine if there is a potential benefit to operating cross-flow turbines with a different preset pitch angle for each camber blade.

Chapter 2

EXPERIMENTAL APPARATUS & METHODS

2.1 Testing Facility

Experiments were conducted in the Harris Hydraulics Lab at the University of Washington using the Alice C. Tyler Flume. This flume is a free-surface water channel, providing control over the flow velocity and water temperature. Consequently, it enables a broad range of Reynolds and Froude numbers for turbine experiments. The flume itself measures 4.6 meters in length, 0.76 meters in width, and 0.7 meters in height. Water temperature was regulated through the utilization of a pool heater. The water temperature was maintained at a constant $38.9°C$, with minor fluctuations of $0.1°C$ being consistently monitored. This monitoring was accomplished by a temperature probe, which was positioned at the entry point of the test section. Flow velocity was controlled by adjusting the pump frequency of the submerged pumps beneath the flume. The specific frequency required for achieving the desired flow velocity varied according to the distinct water properties and depths involved in the experiments.

To measure the velocity of the flow, an acoustic Doppler velocimeter (ADV), the Nortek Vectrino profiler was employed. It operated at a sample rate of 16 Hz, ensuring a consistent and smooth recording of flow velocity. The ADV was strategically positioned at a distance of five turbine diameters upstream from the center shaft of the turbine, situated centrally within the flume. In the experimental setup, the flow velocity of 1.1 meters per second was achieved and maintained with small fluctuations that are considered to be ineffective in the results. Furthermore, the ADV offered valuable insights into the turbulence intensity of the flow, with an average turbulence intensity of approximately 2.43% observed during these experiments. The experimental setup was set closely to match the experiment conditions

from Hunt et al. [5] with one specific Reynolds number.

The Reynolds number calculated from the turbine's diameter with water temperature $38.9°C$ and flow velocity of $1.1m/s$ was found to be 2.81×10^5. The flume's static depth was set at 0.518 meters, while the dynamic depth was measured at 0.481 meters. The Froude number was computed by considering the submergence depth of the turbine, the depth was measured at 0.17 meters from the water surface to the top of the turbine. The resulting Froude number $Fr = \frac{U_\infty}{\sqrt{gH}}$ was found to be 0.85. The blockage ratio was determined by comparing the turbine's swept area to the cross-sectional area of water in the flume. With the turbine's height measured at 0.234 meters, the calculated blockage ratio was 0.11.

2.2 Turbines

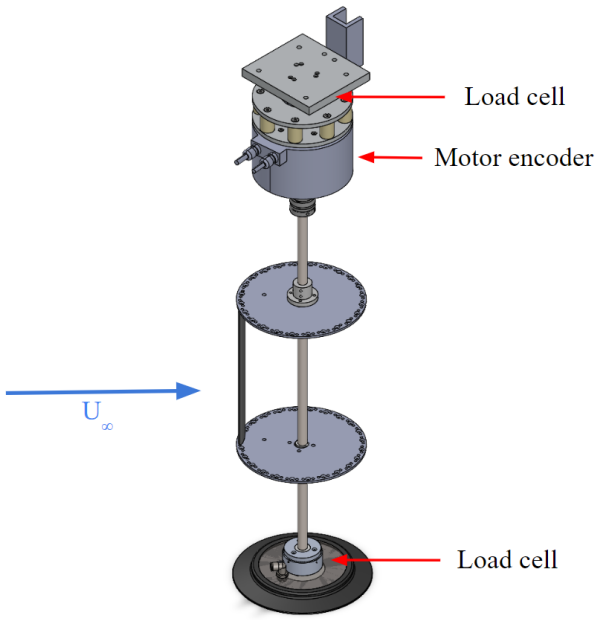

Figure 2.1: Turbine Assembly

The cross-flow turbine used in these experiments is constructed with two circular end plates, a center shaft with a diameter of 1.3 cm, and straight blades featuring an airfoil shape. These

blades are mounted in the locating holes on the end plates. From previous experiments, the struts were found to be a better-supporting structure in terms of performance [9], however, the end plates provide a variety of preset pitch angles without having to manufacture a specific pair of struts for each preset pitch angle. In addition, the end plates were manufactured so the outmost point of the blade at each preset pitch angle has the same distance to the center of the rotation. The choice of straight blades allows the servomotor to collect performance data as a function of azimuthal location. The top end of the shaft is attached to a servomotor (Yaskawa SGMCS-05BC341), which regulates the rotational speed to the desired value, and keeps track of the azimuthal location of the blade and the instantaneous torque and force readings. The torque and force readings were measured from a set of six-axis load cells one on the top of the shaft (ATI Mini45), and one on the bottom of the shaft, and fixed to the bottom of the flume by a suction plate (ATI Mini40). The measurements from the encoder and load cells were recorded by a National Instruments PCIe-6351 card through a custom Simulink model in MATLAB with a sample rate of 1000Hz [5, 10, 6, 11].

The airfoil profiles of the blades are NACA0018 and NACA2418. Based on the virtual camber calculation from Migliore et al. [1], the maximum camber location ranges between $0.4c$ to $0.6c$, with camber varying from 4% to 6%. The NACA2418 airfoil was the largest camber we could get while being able to mount the same airfoil in both directions without change to the supporting pins. The NACA2418 airfoil was mounted in both directions to represent two different camber profiles: positive camber and negative camber relative to the NACA0018 airfoil. The blade's chord length c was 0.0406 m, the turbine's radius R was 0.086 m, and the chord-to-radius ratio was 0.47.

The experiment focused on assessing the blade performance with a single blade across all ranges of tip-speed ratios and preset pitch angles used in the study. The tip-speed ratios used in these experiments were [1.2 1.4 1.6 1.8 2.0 2.1 2.2 2.3 2.4 2.5 2.6 2.8 3.0 3.2]. The preset pitch angles were determined by the mounting holes on the periphery of the end plates with a range from -16° to 4° with a 2° step change. Two different sets of end plates were utilized, allowing for a range of preset pitch angles from -4° to 6° and from 8° to 16° with

2° increments. To minimize drag and ensure consistent performance, the unused locating holes on the end plates were covered with duct tape, as these holes could significantly affect the blade's performance at various tip-speed ratios. During the experiment, a corner of the duct tape that was used to cover the unused mounting holes detached from the end plates, the resulting performance data was 30% off of the actual data. Therefore, the quality of the taping was monitored meticulously throughout all testing sets. The unused mounting holes were covered up by a single piece of duct tape that was stretched and aligned with the circular edge of the end plates. The surface finish of the duct tape must be flat or completely attached to the end plate surface. After the screw was put in to secure the blade, another piece of duct tape was used to cover up the screw and this tape overlapped with the previous duct tape to create a continuous surface finish. During a set of experiments, if the duct tape fell off or showed any sign of imperfection the set of data were deleted and were not used in any data analysis.

2.3 Performance Measurement

The experimental investigation conducted herein focuses on exploring the performance of the cross-flow turbines under controlled conditions. The experiments were conducted at a fixed Reynolds number of 2.81×10^5, maintaining consistency across the trials. Each tip-speed ratio was achieved by the custom MATLAB code, before recording the data for 45 seconds at the sampling frequency of 1000Hz for both blade location and blade force data, the flume was given 15 seconds to reach an equilibrium state from the changing of tip-speed ratio. The data was later post-processed to create the overall time-averaged data, and phase-averaged data based on the blade location.

Turbine performance was evaluated by examining both power production and loading. The coefficient of power C_P is the efficiency of the turbine in terms of how much kinetic energy is provided from the inflow to the amount of energy harvested from the turbine.

$$C_P(\theta) = \frac{\omega\tau(\theta)}{\frac{1}{2}\rho U_\infty^3 2RL} \tag{2.1}$$

Here, τ is the torque and $\tau\omega$ represents the energy converted by the turbine. ρ is the density, L is the blade length or the height of the turbine, and U_∞ is the inflow velocity. The term $2RL$ is the frontal area of the turbine, multiplied by the term U_∞ to get us the mass flow rate through this area, then multiplied by the dynamic pressure of the fluid. The denominator represents the kinetic energy carried by the flow itself. Similarly, the coefficient of force is expressed as,

$$C_F(\theta) = \frac{F(\theta)}{\frac{1}{2}\rho U_\infty^2 2RL} \tag{2.2}$$

where F is the force magnitude that is perpendicular to the turbine shaft, which is the summation of all in-plane force from the two ATI sensors. The time-averaged performance and time-averaged force are denoted as $\overline{C_P}$ and $\overline{C_F}$. Which is the overall time-averaged value of the instantaneous performance and force data at each tip-speed ratio and preset pitch angle.

Blade power and efficiency data were obtained by subtracting the data from a tare run with just the end plates with the same tip-speed ratio range. This approach has been proven effective for these metrics [9]. On the other hand, the force data did not go through the same subtraction, because the force acting on the center shaft will be different with and without the presence of the blade. With the blade, there will be less flow going through the turbine center due to induction. So the force data presented in this study is the force acting on the entire single-blade turbine, the performance data reflects the blade performance without the effects from the end plates.

With the experiment conditions described above, we could directly obtain the performance data and compare whether the change in geometric camber by $\pm 2\%$ has the same magnitude of effect on the performance of the cross-flow turbine when combined with the change in preset pitch angles. Additionally, we could explore whether there exists a better-performing combination of the cambered airfoil and preset pitch angle under a wider range of operating conditions.

Chapter 3

ESTIMATION OF VIRTUAL CAMBER AND INCIDENCE USING THE METHOD OF MIGLIORE

It has been mentioned by Migliore et al. [1], Bianchini et al. [12], and Mandal et al. [13] that the flow curvature significantly impacts the aerodynamic forces of an airfoil. Consequently, the same airfoil in a curvilinear flow field is different when compared to the same airfoil in a rectilinear flow field. The influence due to rotation is mostly reflected in having a different relative inflow velocity along the chord line of the airfoil. Thus, the local effective angle of attack varies along the chord line and it is unique at each point. The terms "virtual camber" and "virtual incidence" were introduced to denote the changes induced by flow rotation.

Following Migliore et al. [3], which employs the conformal mapping method—a transformation of the geometric airfoil from curved flow to its rectilinear flow equivalent—we can derive the virtual incidence and virtual camber. Analysis of the equations derived from Migliore et al. [1] reveals that the relative velocity and the effective angle of attack along the chord line depend on the relative location of the blade to the free stream, the tip-speed ratio, and the chord-to-radius ratio [3]. It is noted that the virtual components are primarily influenced by the chord-to-radius ratio.

The detailed derivation of the set of equations describing the virtual incidence and virtual camber can be found under Migliore and Wolfe's full report with provided computer codes for virtual airfoil transformation [1]. The code was later modified to adapt to our coordinate systems, and the implementation of changes in preset pitch angles, and geometric camber. Notice, that the effects of induction were neglected in the transformation for the virtual component plot in a later discussion. Other considerations including the flow unsteadiness,

blockage, blade-wake interaction, and boundary layer centrifugal effects were important as well but it is outside the scope of this particular study [14]. The output virtual camber is the maximum value of the camber percent along the chord line at each blade location.

The camber line was considered when calculating the virtual camber profile using the conformal mapping technique proposed by Migliore et al. [1]. The NACA 4-digit equation was employed to derive the camber line and airfoil coordinates for the NACA0018 airfoil for this study. Subsequently, this camber line was integrated into the conformal mapping calculation, along with parameters such as the turbine radius, chord length, tip-speed ratio, inflow velocity, blade mounting location, and predetermined preset pitch angles (α_p). However, for the virtual angle of attack, the set of equations provided only took into consideration the leading edge point and trailing edge point, thus, change in the camber line does not affect the virtual AOA.

We explore the influence of preset pitch (α_p) on estimates of virtual camber γ_r (Fig. 3.1) and angle of attack α_r (Fig. 3.4) as calculated using the method of Migliore [1]. As noted by Athair et al. [4] and Migliore et al. [3], virtual geometry is very sensitive to the tip-speed ratio and the change in chord-to-radius. The sensitivity of the virtual component due to the change in the nominal condition was studied again to justify the selection of the cambered airfoil used in the later experiments.

The previous study has a more complete study of the impact of the chord-to-radius ratio [4], this study, calculations conducted here were for the experimental turbine with a fixed chord-to-radius ratio of 0.47. Given that altering the mounting location affects the relative radius of the turbine, in this study, the mounting location was standardized to the quarter chord position. The conformal mapping calculation generated the camber percentage as a function of the blade's azimuthal location. The virtual camber, determined as the difference between the total camber and the geometric camber inherent to the airfoil, represents the camber component induced by the blade's rotational motion within the flow field.

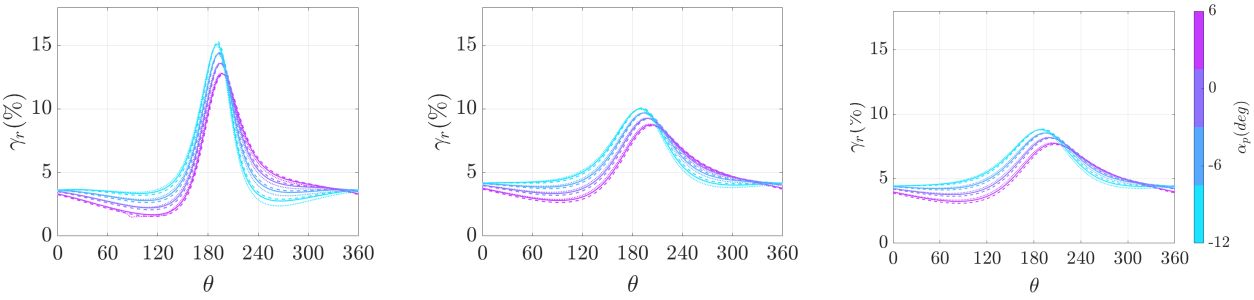

(a) $\lambda = 1.6$ (b) $\lambda = 2.4$ (c) $\lambda = 3$

Figure 3.1: Comparison of the virtual camber due to rotation at different tip-speed ratios at four different preset pitch angles with $\frac{c}{R} = 0.47$. The preset pitch angles range from $-6°$ to $12°$ at $6°$ increments. The line types represent different geometric camber as following ..... $\gamma_g = +2\%$, —— $\gamma_g = 0\%$, – – – $\gamma_g = -2\%$.

As the TSR increases, the peak of the virtual camber decreases. The geometric camber does not have a strong influence on the resulting virtual camber. An increase in the preset pitch angle causes a delay to the peak magnitude of the γ_r. Also, an increase in the preset pitch angle causes a lower magnitude of γ_r in the upstream and a higher γ_r in the downstream. Notice the change in the virtual camber corresponds to a change in preset pitch angle of $-6°$, which is roughly 1.5% across all TSR tested, and the effects of preset pitch angle are significant across all TSR. However, the change in the geometric camber does not have the same magnitude of the effects: a change in the camber with 2% magnitude in either direction would lead to a change in the virtual camber with a magnitude much less than 0.3% in the same direction as the geometric camber. The representation of positive and negative camber through dotted and dashed lines respectively demonstrates that augmenting geometric camber minimally affects virtual camber.

In essence, under a constant chord-to-radius ratio, the virtual camber calculated from Miglore's method appears more responsive to alterations in preset pitch angles compared to changes in geometric camber. Through the same calculation, a higher chord-to-radius ratio

would make the impact of geometric camber more obvious but still not as significant as the preset pitch angle across all TSR.

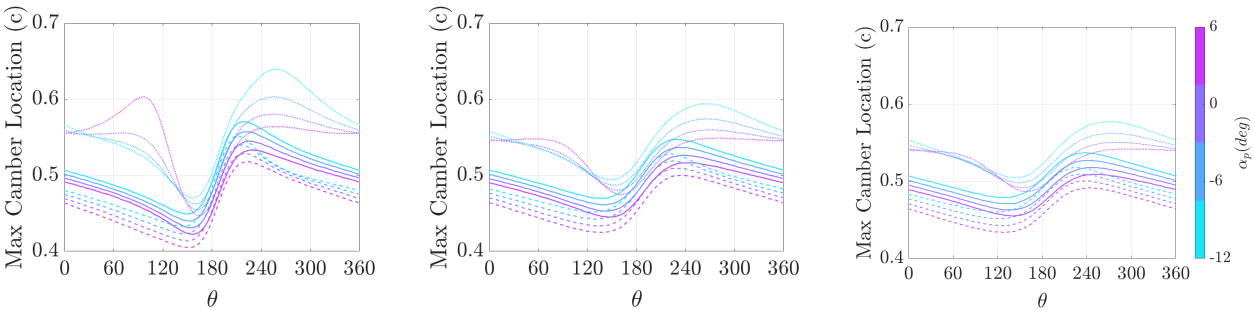

(a) $\lambda = 1.8$ (b) $\lambda = 2.4$ (c) $\lambda = 3$

Figure 3.2: Comparison of the maximum camber location at different tip-speed ratios at four different preset pitch angles with $\frac{c}{R} = 0.47$. The preset pitch angles range from $-6°$ to $12°$ at $6°$ increments. The line types represent different geometric camber as following ..... $\gamma_g = +2\%$, —— $\gamma_g = 0\%$, − − − $\gamma_g = -2\%$.

Fig. 3.2 shows the range of maximum camber location across three different TSRs in terms of the chord length from the leading edge. The maximum camber location varies within the range of $0.4c$ to $0.6c$. The increase in the TSR decreases the range of the variation. An increase in the preset pitch angle brings the maximum camber location forward. The positive camber shifts the maximum location backward, the negative camber shifts the maximum camber location forwards. The positive camber has a more dramatic change to the maximum camber location when compared to the negative camber. Overall, the change in the maximum camber location is more sensitive to the change in the geometric camber than the change in the preset pitch angle or tip-speed ratio.

From the previous examination of the virtual transformation [4], it was found the average magnitude of change in virtual camber by having a change of preset pitch angle of $6°$ over various TSRs from the calculation is 4% to 6%. Earlier studies chose to utilize a $6°$ preset

pitch angle as it was found to be close to optimum for a range of Reynolds numbers when using symmetric airfoil (zero camber foils) [5]. Fig. 3.1 illustrates pitch angle variations in 6 degree increments, while virtual camber changes in magnitude occur at around 1.5%. This observation prompted an investigation into adding a 2% geometric camber to the symmetrical airfoil and assessing its impact on the virtual camber, thus, a NACA2418 airfoil was designed to fit in the current turbine configuration with the ability to be tested under different preset pitch angles [4]. The airfoil NACA2418 was chosen through the virtual analysis showing the maximum camber location varied from $0.4c$ to $0.6c$. The 2% camber was mainly limited by the maximum amount the airfoil could bend for the airfoil to be mounted the same way in both directions.

Differing from the calculation of the virtual camber, the computation of the virtual angle of attack considers solely the starting and ending points of the airfoil's chord line. Consequently, the alteration in geometric camber doesn't mathematically induce a virtual camber component on the airfoil. The nominal angle of attack shows the relative angle between the relative flow and the blade chord line disregarding the effects of induction. It has been shown the nominal angle of attack depends on the blade location, the inflow velocity, and the preset pitch angle Eq. 1.2. The preset pitch angle adds a constant value across all θ, and as TSR increases the magnitude of the relative flow velocity increases, thus, decreasing the peak and the average nominal angle of attack.

From Fig. 3.4, an increase in the preset pitch angle delays the peak magnitude of α_r. Additionally, it results in a lower upstream α_r and a higher downstream α_r. The reduced α_r in the upstream region, particularly around $\theta = 120°$, where the relative angle between the airfoil and the flow is approximately 3°, may extend the power extraction cycle. As depicted in Fig. 3.4, a higher preset pitch angle accelerates the recovery in α_r. A higher α_r in the downstream could potentially lead to an earlier recovery cycle and decrease energy loss during the detrimental performance cycle in the downstream. This is saying the change in preset pitch angle has similar effects on the upstream region across all TSR, but as TSR increases the effects of the change in preset pitch angle become less obvious in the downstream region.

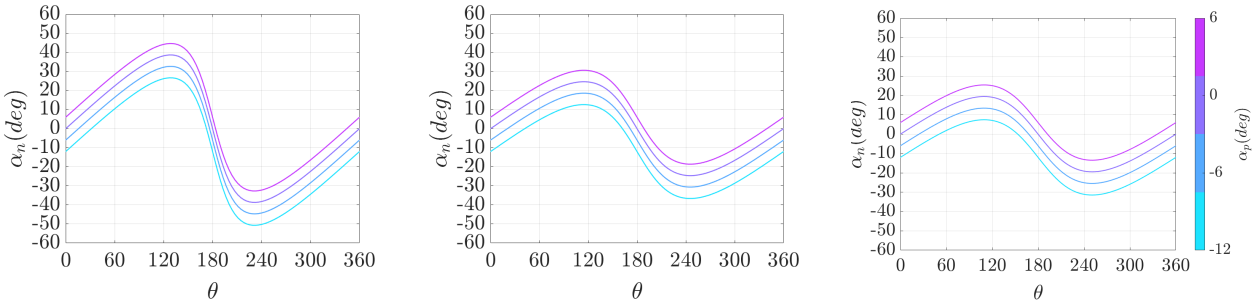

(a) $\lambda = 1.6$ (b) $\lambda = 2.4$ (c) $\lambda = 3$

Figure 3.3: Comparison of the nominal angle of attack at different preset pitch angles with a fixed chord-to-radius ratio of 0.47.

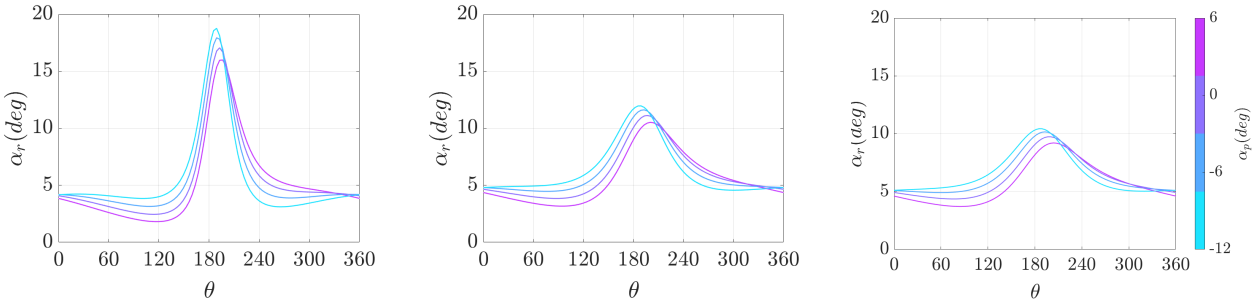

(a) $\lambda = 1.6$ (b) $\lambda = 2.4$ (c) $\lambda = 3$

Figure 3.4: Comparison of the angle of attack due to rotation at different tip-speed ratios with a fixed chord-to-radius ratio of 0.47. The induced angle of attack is not affected by the change in geometric camber from the method proposed by Migliore et al. [1].

Chapter 4

RESULTS AND DISCUSSION

The performance data were collected with all three different camber airfoils, the positive camber $\gamma_g = 2\%$, negative camber $\gamma_g = -2\%$, and the symmetric airfoil. The same cambered airfoil was mounted in both directions to represent the two different camber directions. The preset pitch angle ranges from -16° to 4° with the step of 2°. The TSR ranges from 1.2 to 3.2 with a fixed inflow velocity of $1.1m/s$.

As shown in Fig. 4.1, the time-averaged data collected from the experiment were plotted as a contour map, with the middle one representing the symmetric airfoil case, while the two plots on the side showing the difference between the camber airfoil case and the symmetric airfoil case. The red dots on the contour map are the optimal performance case for each airfoil.

The optimal preset pitch angle for the symmetrical airfoil is -8°, with a TSR of 3.0. This is slightly different when compared to previous experiments showing the optimal $\alpha_p = -6^\circ$ likely due to a higher Reynolds number used in this specific experiment [5]. The optimal preset pitch angle for each camber airfoil case is -8° except for $\gamma_g = +2\%$ which has a higher α_p equal to -6°. The optimal performance of the three camber cases shares the same optimal TSR at $\lambda = 3.0$.

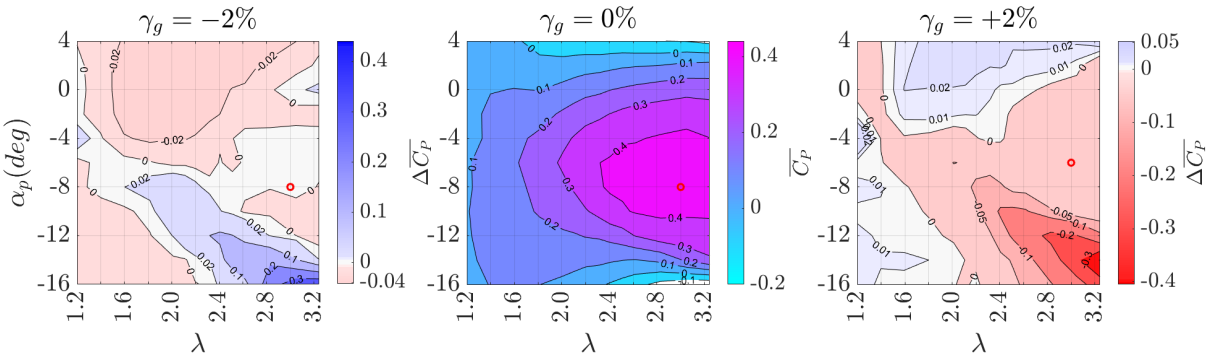

Figure 4.1: Comparison of the time-averaged coefficient of power for different geometric camber airfoils. The middle contour shows the $\overline{C_P}$ for the symmetrical airfoil ($\gamma_g = 0\%$). The left contour shows the $\overline{C_P}$ difference compared to the symmetric foil for negative camber ($\gamma_g = -2\%$), and the right contour shows the $\overline{C_P}$ difference compared to the symmetric foil for positive camber ($\gamma_g = +2\%$).

The performance contour shows the $\gamma_g = 0\%$ case performs closely to the optimal value within the operating condition of TSR ranges from 2.4 to 3.2 and preset pitch angle ranges from $-10°$ to $-4°$. The optimal performance of the three camber cases is also similar. The optimal $\overline{C_P}$ for the symmetrical airfoil is 0.4411 with $\alpha_p = -8°$. The difference between $\gamma_g = -2\%$ case and symmetric foil in $\overline{C_P}$ is 0.005 with negative camber case performing 1.25% better at 0.4466 with $\alpha_p = -8°$. The difference between $\gamma_g = +2\%$ and the symmetric foil in $\overline{C_P}$ is 0.01 with the positive camber case performing 2.7% worse at 0.4292 with $\alpha_p = -6°$.

The negative camber airfoil with $\gamma_g = -2\%$ shows an increase in $\overline{C_P}$ in the region where α_p ranges from $-8°$ to $-16°$ and TSR ranges from 1.8 to 3.2, this region corresponds to a low α_p and at high λ. This increase is mostly reflected in the region where the symmetrical case has net zero or negative efficiency. The change in $\overline{C_P}$ in this region could mean the turbine can operate at extremely low preset pitch angles at a high TSR while being able to produce energy, but the preset pitch angle cannot be changed during the operation with our fixed preset pitch angle configuration, and a preset pitch angle close to the optimal value will

still be the favored choice. At higher α_p ranges from -4° to 4° across all TSR and when α_p ranges from -16° to -8° when TSR ranges from 1.2 to 2.0 the contour is showing a minor decrease in $\overline{C_P}$ with an average magnitude of change of 0.02 in $\overline{C_P}$. This shows the negative camber airfoil case has almost identical performance over the operating conditions tested. Showing an 0.4 increase in $\overline{C_P}$ in regions with high TSRs and low preset pitch angles when the symmetric foil shows detrimental performance, results in a net positive performance with a magnitude of 0.1 to 0.2.

On the other hand, the positive camber case with $\gamma_g = +2\%$ shows an opposite trend as the negative camber case. The positive camber case has a detrimental performance in the region where the negative camber case shows an increase in $\overline{C_P}$. While showing an increase in $\overline{C_P}$ with the magnitude of 0.02 in the region where negative camber shows a decrease in $\overline{C_P}$ of magnitude -0.02. The net $\overline{C_P}$ in this region still shows the turbine has zero efficiency or negative performance with the 0.02 increase brought by the positive camber airfoil. In the region when α_p ranges from -16° to -8° and TSR ranges from 1.8 to 3.2, the positive camber case shows a decrease in the performance with magnitude up to 0.4 when compared to the symmetric foil.

Fig. 4.2 shows a summary of the optimal preset pitch angles for each camber airfoil profile. The optimal preset pitch angles at TSR range from 1.2 to 1.6 fluctuate widely due to the turbine not exhibiting positive performance in this TSR range. The blade oscillates between weak attached flow and detached flow, resulting in the absence of a representative optimal preset pitch angle for turbine performance.

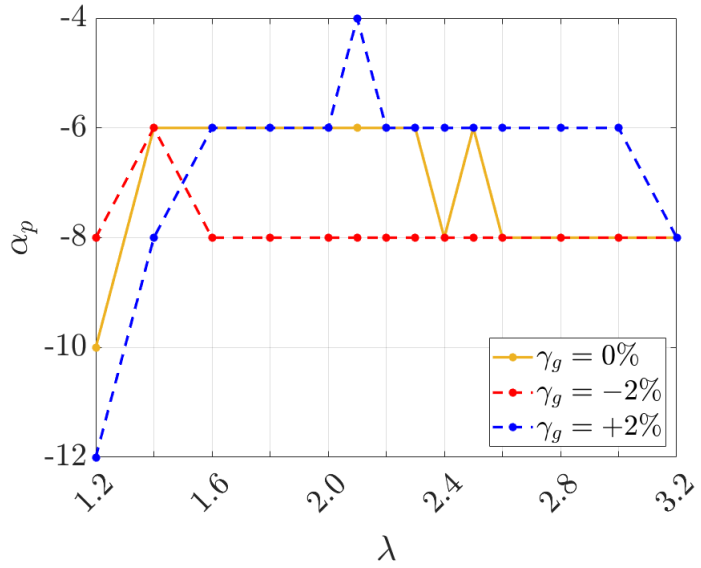

Figure 4.2: Optimal preset pitch angle at different TSR for each camber foil.

In the TSR range from 1.6 to 3.2, the optimal preset pitch angle for each camber profile is consistent with changing TSR. There are small changes for the symmetric airfoil at TSR = 2.4 and slight variations for the positive camber at TSR = 2.1. However, due to the limitations of experimental resolution in the preset pitch angles, which have 2° increments, these small fluctuations cannot accurately represent the absolute optimal preset pitch angle. Instead, they indicate the optimal angle within the tested range of α_p.

The change in TSR has little effect on the optimal preset pitch angle for each camber airfoil. While the positive camber shifts the optimal preset pitch to a higher value at $-6°$, the negative camber shifts the optimal angle to a lower value at $-8°$ for most TSRs. The optimal preset pitch angle for the symmetric fluctuates between the two camber cases at $-6°$ at lower TSRs and $-8°$ at higher TSRs.

On top of the time-averaged data, we explore the phase-averaged performance of the single-bladed turbine and are thus able to correspond torque to a specific blade phase. From Fig. 4.3, we can see the phase-averaged coefficient of power plotted against the azimuthal

location of the blade θ for different TSRs, preset pitch angles, and camber profiles. Our sign convention for preset pitch angle is defined according to this trend, the increase in preset pitch angles corresponding to an increase in peak C_P in the upstream.

An increase in the TSR across all cases increases the peak performance upstream, while the downstream performance is not significantly affected by the change in TSR. Also, the peak performance phase location is delayed as the TSR increases. At low TSR, when $\lambda = 1.6$, the peak performance has a similar magnitude across several preset pitch angles. At higher TSR, when $\lambda = 2.4$, $\lambda = 3.0$, the peak performance increases as α_p increases. For cases when $\lambda = 1.6$, $\lambda = 2.4$, an increase in preset pitch angle brings the peak performance to an earlier phase, at $\lambda = 3.0$ the peak performance location does not vary as preset pitch angles vary. Notice the best-performing preset pitch angle upstream does not have the best performance downstream but the worst.

As for different camber airfoils, the negative camber decreases the peak performance upstream of the cycle and increases peak C_P downstream when compared to the symmetric foil. The positive camber increases the peak C_P upstream and has a detrimental performance downstream when compared to the symmetric foil as seen by Athair et al. [4]. The positive camber and negative camber have the opposite effect on the peak C_P at different phases. The same trend was used for the sign of our camber, a positive camber corresponds to an increase in the upstream peak C_P, and a negative camber means a decrease in peak C_P in the upstream [4].

While increasing the preset pitch angle up to $-4°$ or having a positive camber could enhance the performance upstream, the overall performance is critically determined by the downstream performance. Most of the time, having a higher preset pitch angle means more detrimental performance downstream. Having a negative camber airfoil could turn the detrimental performance downstream into a power-producing region with some sacrifice in the peak performance upstream. This phase-averaged data reveals that overall turbine performance depends on a balance between upstream and downstream performance.

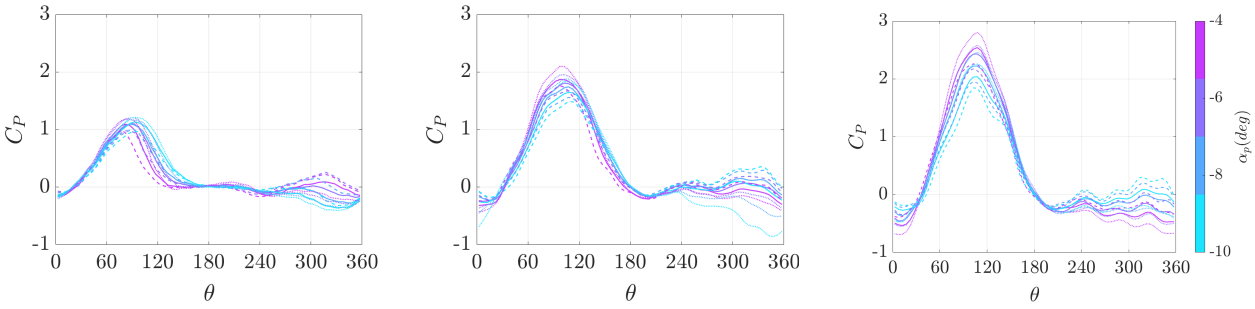

(a) $\lambda = 1.6$ (b) $\lambda = 2.4$ (c) $\lambda = 3.0$

Figure 4.3: Comparison of the phase-averaged blade performance for different camber airfoils at four different preset pitch angles. The line types represent different geometric camber as following ..... $\gamma_g = +2\%$, —— $\gamma_g = 0\%$, − − − $\gamma_g = -2\%$.

From previous observations, the overall average performance of the turbine is not affected a lot by changes in the camber profile, while the change in the camber does show a difference in the change in the upstream region and downstream region. Now the time-averaged data (Fig. 4.4) shows the overall average performance is now separated as upstream region and downstream. From the symmetric foil, the optimal point which is at $\lambda = 3.0$ and $\alpha_p = -8°$ does not correspond to the highest $\overline{C_P}$ in the upstream, and it does not correspond to the least detrimental point in the downstream either. The best-performing condition for the upstream region is at $\lambda = 3.2$ and when $\alpha_p = -4°$, note the optimal preset pitch angle and optimal TSR are different compared to the preset pitch angle and TSR for the overall optimal time-averaged performance. The downstream region has worse performance at a higher TSR with the extreme value of α_p having a negative performance. Thus, the turbine performance depends on the combination of the upstream and downstream performance. In other words, a well-performing upstream region with a less detrimental downstream performance makes the optimal condition [11].

For $\gamma_g = -2\%$, the blade performs slightly worse in the upstream region for all combina-

tions of preset pitch angles and TSR, with a change in performance of -0.1 at the optimal point. In the downstream, the negative camber blade performs slightly better at higher TSR and low preset pitch angles, with an increase in $\overline{C_P}$ with a magnitude of 0.1 at the optimal point. With this being said, the negative change in $\overline{C_P}$ in the upstream is canceled out by the positive change in $\overline{C_P}$ in the downstream, but not completely. The negative camber airfoil has a small net gain in the overall performance. For $\gamma_g = +2\%$, the blade performance is better in the upstream region with a magnitude of 0.05 to 0.1 for all combinations of λ and α_p, with a positive change of 0.08 in $\overline{C_P}$ at the optimal point. In the downstream, the positive camber blade performs worse than the symmetric foil, with a negative change of 0.1 at the optimal point. This sums up to have a negative net gain in $\overline{C_P}$ when compared to a symmetric airfoil. Overall, the positive camber increases the $\overline{C_P}$ in the upstream region, while decreasing the $\overline{C_P}$ in the downstream region. The negative camber has the opposite effect on the performance of the turbine, which decreases the $\overline{C_P}$ in the upstream region and increases the $\overline{C_P}$ in the downstream region. The net change for positive camber results in a decrease in the overall performance, while the negative camber provides a slightly better performance overall when compared to the symmetric airfoil.

Through the symmetrical airfoil, the upstream performance shows there exists one optimal preset pitch angle at higher TSR. As the preset pitch angle approaches the extreme, the highest or the lowest value the blade will have no ability to extract energy from the flow field. As the preset pitch angle approaches the optimal value, the blade performance increases. In the downstream, the same trends were observed the downstream performance is more sensitive to the preset pitch angle at higher TSRs, and as the preset pitch angle approaches the extreme ends the blade has detrimental performance. The upstream performance for both camber airfoils is not sensitive to the preset pitch value, but rather dependent on the TSR. At the lower TSRs, the negative camber airfoil has a negative performance when compared to the symmetric foil, and the upstream performance gets worse as the TSR increases. The positive camber airfoil has the opposite trend, at lower TSR the positive camber airfoil has a performance gain of 0.05, and as TSR increases the performance gain reaches 0.1 and

fluctuates unevenly depending on the preset pitch angle.

The downstream performance however is extremely sensitive to the preset pitch angle at higher TSRs. For both camber airfoils, the change in the performance at the lower TSR region is close to zero when compared to the symmetric foil, it is also insensitive to the preset pitch angle. At higher TSRs, when $\lambda \geq 2.4$, the negative camber airfoil shows an increase in the $\overline{C_P}$ with a magnitude of 0.1 around the optimal point compared to the symmetric foil. This increase in $\overline{C_P}$ increases as the preset pitch angle approaches -16° with the magnitude of 0.8 at most. The positive camber shows the opposite trend, at the optimal point the positive camber has a negative change in $\overline{C_P}$ with a magnitude of 0.1, and the negative change in $\overline{C_P}$ increases up to 0.8 at most.

The blade performance upstream is more sensitive to the preset pitch angles at higher TSRs, with one optimal preset pitch angle for each TSR when the TSR is higher than 2.4. The upstream performance for both camber airfoils does not depend on the preset pitch angle but on the TSR. The negative camber exhibits a negative change in $\overline{C_P}$ upstream, and the change magnitude increases as TSR rises. In contrast, the positive camber shows an increase in upstream $\overline{C_P}$, and its magnitude increases with higher TSR values. Blade performance downstream is more sensitive to the preset pitch angle at higher TSRs as well. At higher TSRs, when α_p approaches the extreme value, the blade exhibits detrimental performance. However, using a negative camber airfoil can transform the detrimental performance at high TSR, with α_p ranging from -16° to -8°, into a power-producing region.

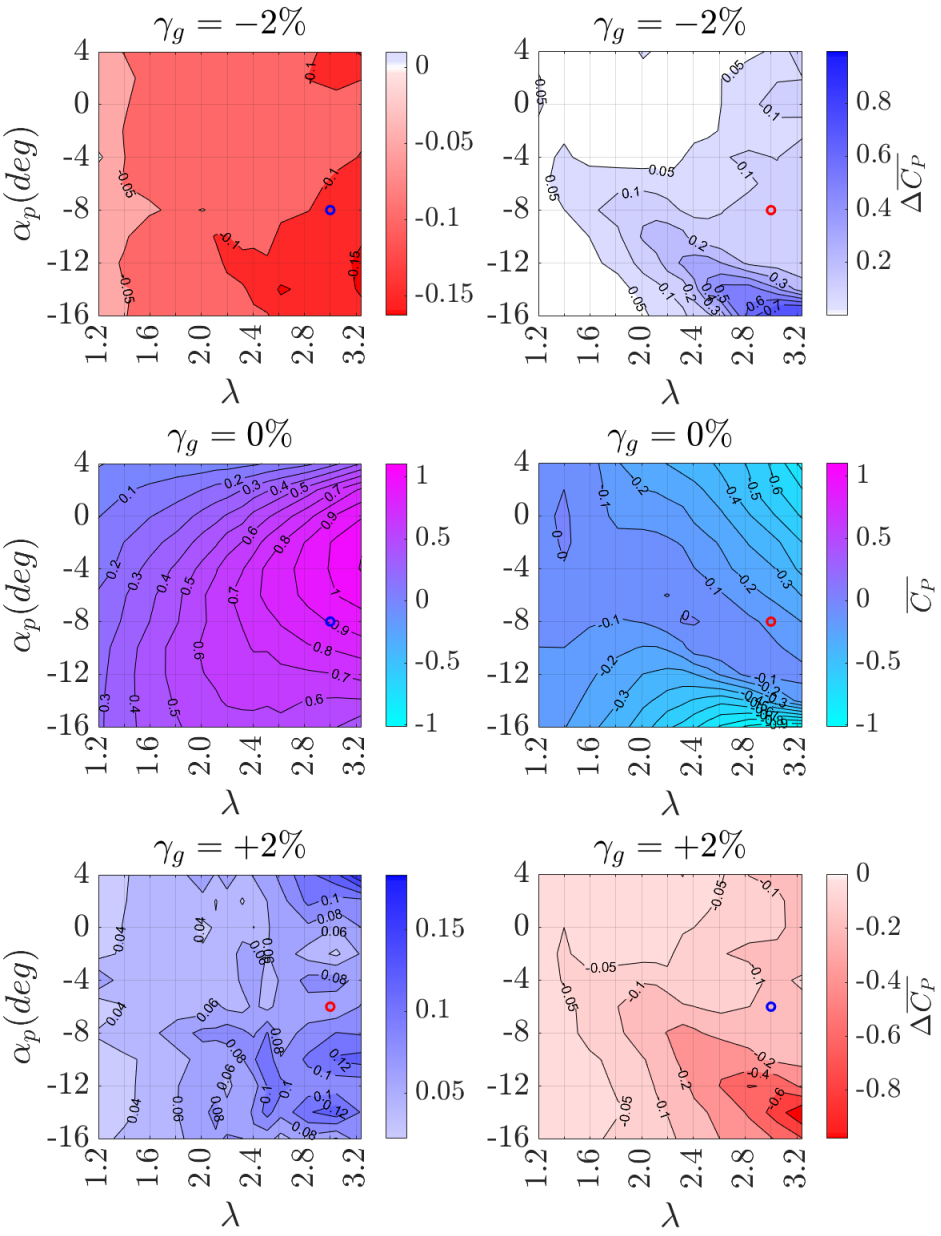

Figure 4.4: Contour plots for the time-averaged coefficient of power upstream (left column) and downstream (right column) for each geometric camber airfoil. The coefficient of power contours for $\gamma_g = 0\%$ is shown in the middle. The top and bottom contours correspond to the difference in $\overline{C_P}$ for cambered foils when compared to the $\gamma_g = 0\%$ case.

Through this analysis of overall time-averaged performance data and the separation of upstream and downstream $\overline{C_P}$ contours, no data suggests an increase in the overall performance of the turbine by changing the camber percent with a magnitude of 2%, either positive or negative. From the phase-averaged performance, the contribution of detrimental performance in the downstream region shows determinant effects on the overall turbine performance. Alternatively, the better-performing downstream blade corresponds to the better-performing blade overall under the given testing conditions. The upstream performance is quite insensitive to preset pitch but that downstream is sensitive. The differences between each camber airfoil in the downstream performance occur at the lower preset pitch.

Another important characteristic of the cross-flow turbines is the structural loading that it is under. Since the blade cuts the inflow with a wide range of angles of attack, the forcing on the blade and the entire structure varies significantly, which often causes challenges related to the size of support structures and structural fatigue. Fig. 4.5 shows the time-averaged coefficient of force ($\overline{C_F}$), we can directly observe the change in the $\overline{C_F}$ as a result of the change in camber percent to the blade. Also, from the symmetrical airfoil, the average $\overline{C_F}$ grows as both the TSR and preset pitch angle increase. The extreme operating conditions of the blade caused an increase in the $\overline{C_F}$ while having a decrease in the $\overline{C_P}$ in these regions.

We observe from the contour representing the symmetric airfoil that the time-averaged coefficient of force is not sensitive to the preset pitch angle until a higher-end TSR is reached. When TSR is less than 2.4, $\overline{C_F}$ remains unchanged with preset pitch angles. At higher TSRs, $\overline{C_F}$ stays approximately constant for α_p ranges from -12° to -4° and increases rapidly at extreme values of preset pitch angle.

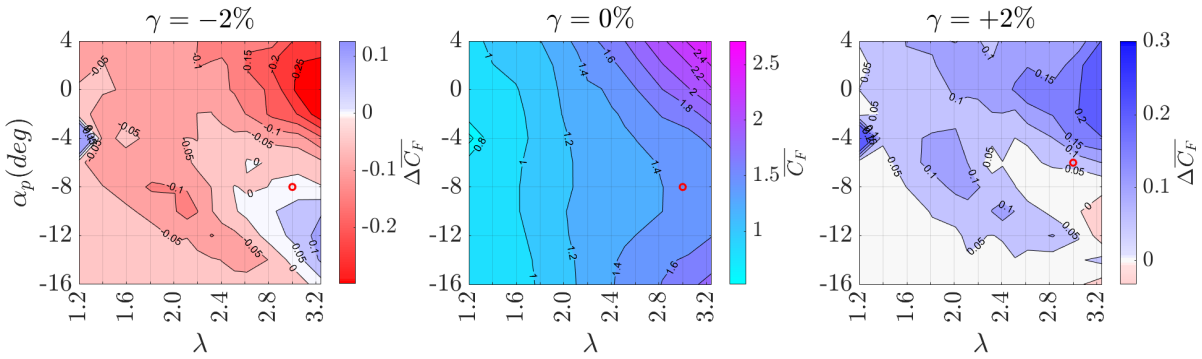

Figure 4.5: Comparison of the time-average coefficient of force for different geometric camber airfoils. The middle contour shows the $\overline{C_F}$ for the symmetrical airfoil $\gamma_g = 0\%$. The left contour shows the $\overline{C_F}$ difference compared to the symmetric foil for $\gamma_g = -2\%$, and the right contour shows the $\overline{C_F}$ difference compared to the symmetric foil for $\gamma_g = 2\%$.

Regarding the change in $\overline{C_F}$ with variations in blade camber, opposite camber airfoils have opposite effects. The $\gamma_g = -2\%$ case reduces the coefficient of force in most regions compared to the symmetric foil, except at the optimal operating condition where the negative camber profile closely matches the symmetric foil. $\overline{C_F}$ is smaller at lower preset pitch angles for all TSRs for the negative camber airfoil, except for $\lambda = 3.2$, where higher preset pitch angles exhibit a significant drop in $\overline{C_F}$ in the top right corner of the contour.

In the case of positive camber ($\gamma_g = +2\%$), $\overline{C_F}$ increases in most regions, with minimal change at lower α_p across all λ ranges. At the optimal condition for the positive camber case, there is an increase in the coefficient of force with a magnitude of 0.05. Comparing this contour plot to the $\overline{C_P}$ contour (Fig. 4.1) when $\gamma_g = +2\%$, at lower α_p, the change in $\overline{C_F}$ is close to zero, while the positive camber airfoil experiences a significant performance drop. At higher α_p, the positive camber airfoil gains performance, with a magnitude of 0.01, and an increment in $\overline{C_F}$ with a magnitude of 0.15. In the negative camber case, at lower preset pitch angles, there is a decrease in force loading with a magnitude of 0.05, while the change in $\overline{C_P}$ is positive if not zero. At higher α_p, the negative camber case experiences a

negligible decrease in $\overline{C_P}$ with a magnitude of 0.02, while benefiting from a significant drop in $\overline{C_F}$, especially at the higher end of the TSR.

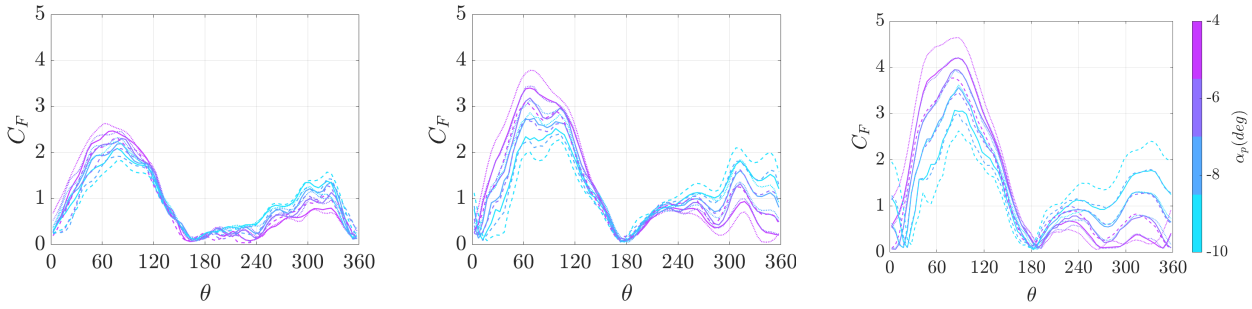

(a) $\lambda = 1.6$ (b) $\lambda = 2.4$ (c) $\lambda = 3.0$

Figure 4.6: Comparison of the phase-averaged coefficient of force for different camber airfoils at four different preset pitch angles. The line types represent different geometric camber as following ..... $\gamma_g = +2\%$, —— $\gamma_g = 0\%$, – – – $\gamma_g = -2\%$.

Similar to the phase-average performance (Fig. 4.3), Fig. 4.6 depicts the phase-averaged coefficient of force (C_F) as a function of the blade azimuthal position θ. The coefficient of force plots exhibit trends similar to those observed in the coefficient of power plots. An increase in the TSR results in an elevated peak C_F. At low TSR, C_F is more dependent on the camber profile than the change in preset pitch angle. Conversely, at higher TSRs, C_F becomes more sensitive to the camber profile upstream and the preset pitch angle downstream.

In the upstream section, a positive camber profile corresponds to a higher upstream C_F and an increase in the preset pitch angle in the upstream leads to an increase in C_F. Where an increase in the preset pitch angle and camber percent translates to a higher peak C_F upstream. On the downstream side, similar effects from the preset pitch angles and camber percent on the coefficient of force are observed when compared to the phase-averaged performance (Fig. 4.3). The positive camber, exhibiting the highest peak C_F in the upstream, has the lowest C_F in the downstream for all preset pitch angles in all TSRs. Conversely, the

negative camber, with the lowest C_F in the upstream, now displays the highest C_F in the downstream for all cases. The symmetric airfoil falls between the other two camber profiles, lacking the highest C_F in either the upstream or downstream. These trends suggest a direct correlation between the coefficient of power and the coefficient of force. In other words, a better-performing blade experiences higher force.

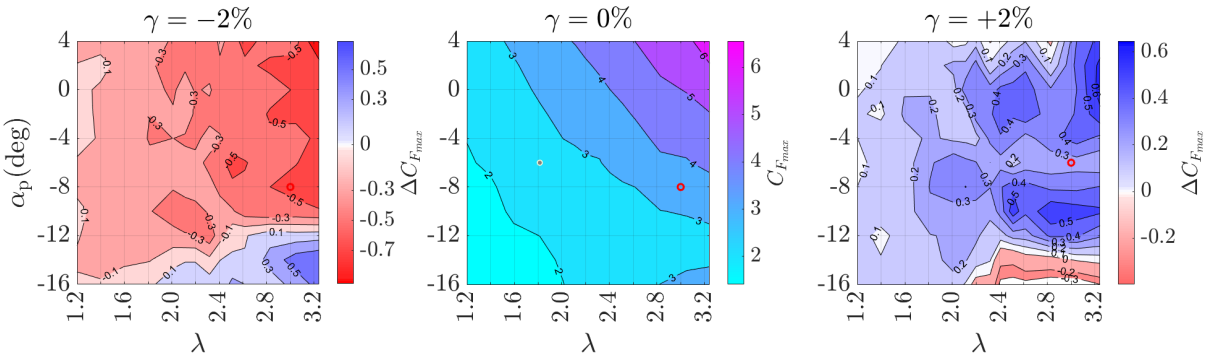

Figure 4.7: Comparison of the maximum coefficient of force throughout a cycle for different geometric camber airfoils. The middle contour shows the C_{Fmax} for the symmetrical airfoil $\gamma_g = 0\%$. The left contour shows the C_{Fmax} difference compared to the symmetric foil for $\gamma_g = -2\%$, and the right contour shows the C_{Fmax} difference compared to the symmetric foil for $\gamma_g = +2\%$.

Another metric of importance is the maximum force, as it is related to the overturning moment on cantilevered turbines. Fig. 4.7 shows the maximum coefficient of force (C_{Fmax}) as a function of TSR and preset pitch. From the symmetric airfoil, the $C_{F_{max}}$ increases with an increase in both the TSRs and the preset pitch angles. Regarding cambered airfoils, the change in maximum loading is just as dependent on the preset pitch as the symmetric foils since the cambered plots show deviation from the symmetric foil. The region where negative camber exhibits an increase in maximum loading, particularly when $\alpha_p = -16°$ and λ ranges from 2.4 to 3.2, corresponds to the region where negative camber demonstrates

improved performance while positive camber results in detrimental performance compared to the symmetric foil.

Comparing the $C_{F_{max}}$ for the negative camber to the symmetric foil, there is a decrease in most operating regions except for the lowest α_p with higher λ. The decrease in $C_{F_{max}}$ ranges from -11% to -17% for most regions, with a magnitude of -16% at the optimal operating point compared to the symmetric airfoil. In the positive camber case, there is an increase in the $C_{F_{max}}$ in most regions, with a magnitude ranging from 5% to 10% compared to the symmetric foil. At the optimal operating condition, there is an increase in the $C_{F_{max}}$ with a magnitude of 6% compared to the symmetric airfoil. Differing from the time-averaged $\overline{C_F}$ contour, the $C_{F_{max}}$ contour distinctly indicates a decrease in the maximum structural loading the blade experiences for negative camber foil compared to the symmetric foil, and this decrease is notably less pronounced when compared to the positive camber foil.

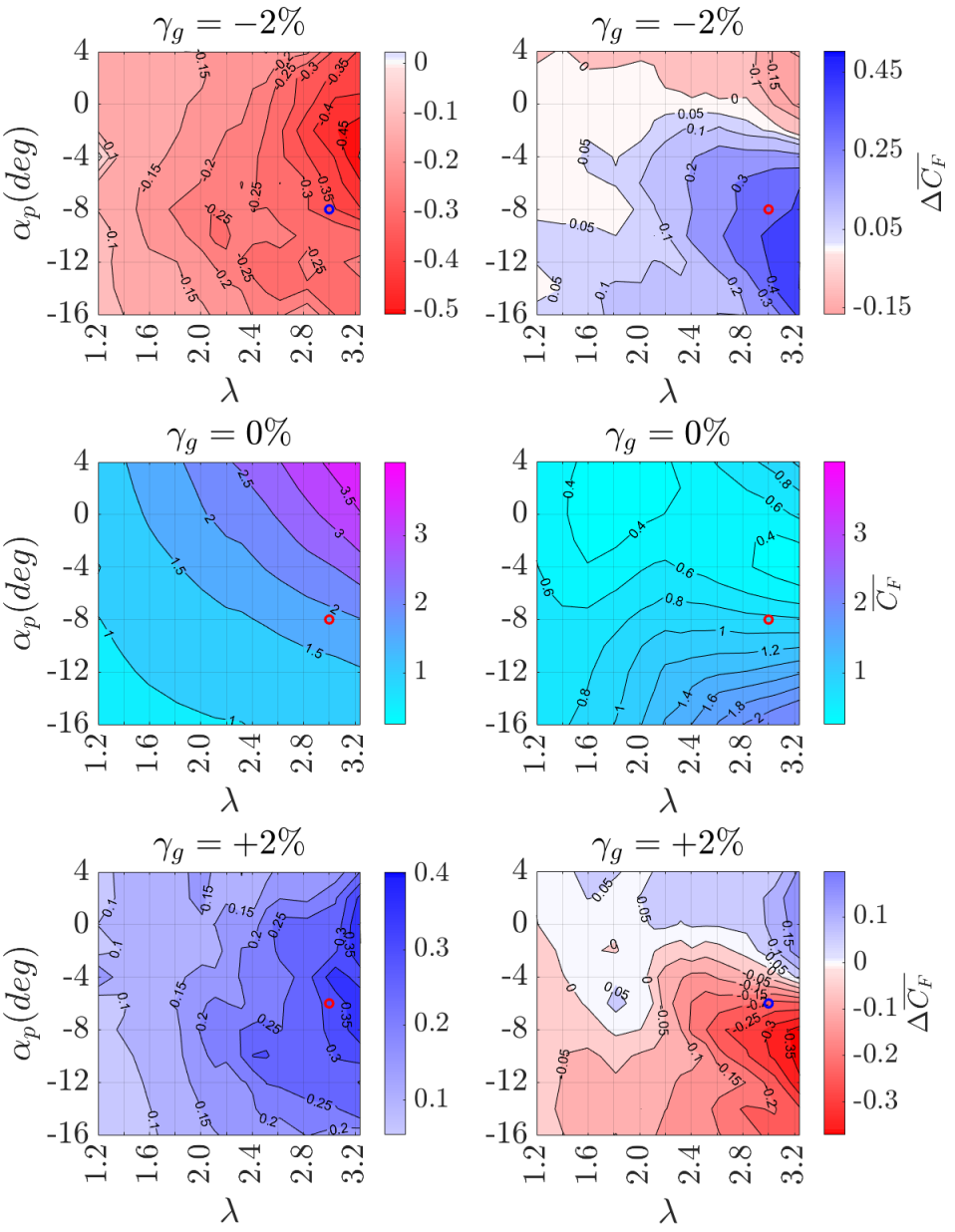

Figure 4.8: Contour plots for the time-averaged coefficient of force upstream and downstream for each geometric camber airfoil. The time-averaged coefficient of force contours for $\gamma_g = 0\%$ are shown in the middle. The top and bottom contours correspond to the difference in $\overline{C_F}$ when compared to the $\gamma_g = 0\%$ case. The left column corresponds to the upstream region, the right column corresponds to the downstream region.

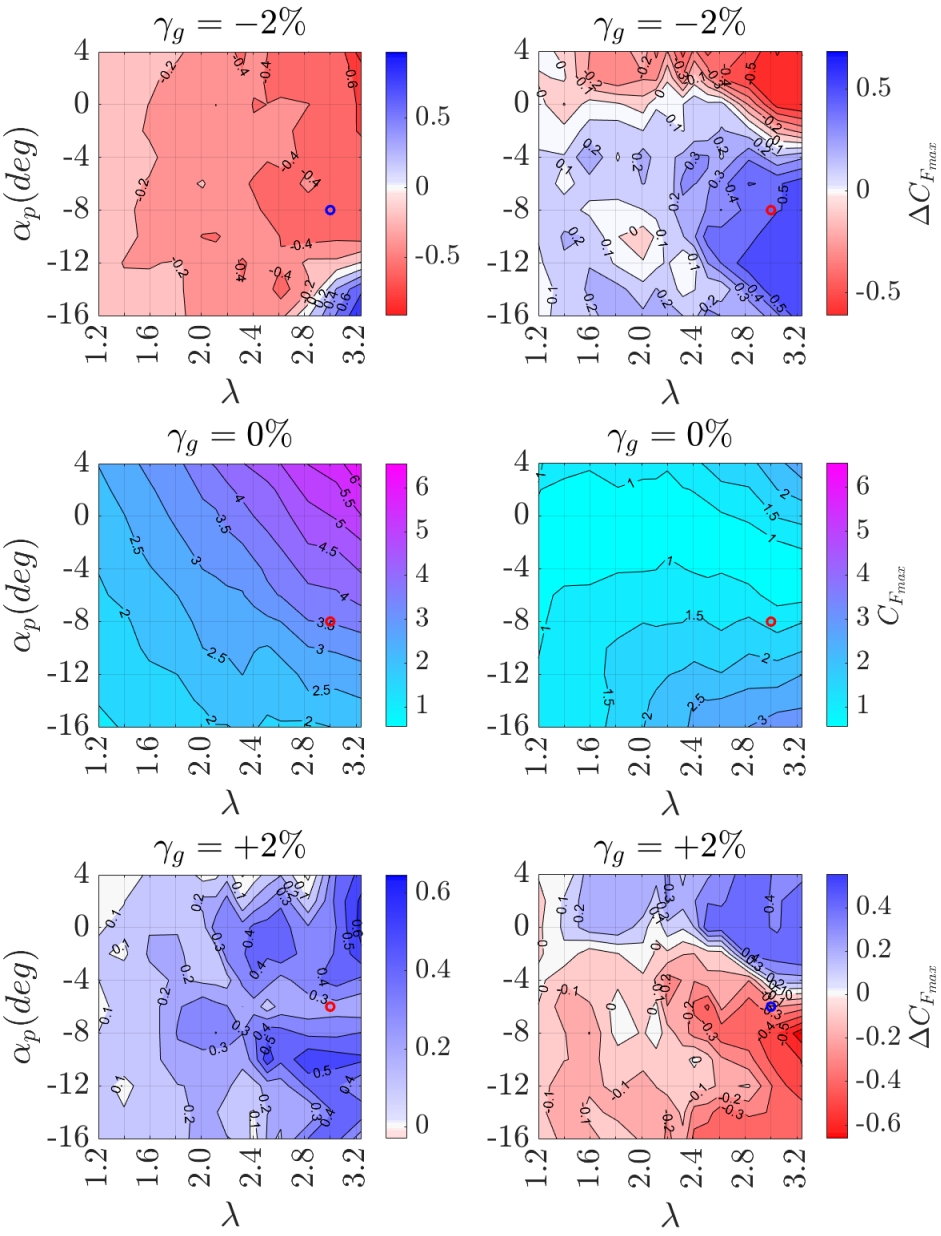

Figure 4.9: Contour plots for the maximum coefficient of force upstream and downstream for each geometric camber airfoil. The maximum coefficient of force contours for $\gamma_g = 0\%$ are shown in the middle. The top and bottom contours correspond to the difference in C_{Fmax} when compared to the $\gamma_g = 0\%$ case. The left column corresponds to the upstream region, the right column corresponds to the downstream region.

Knowing the camber airfoils have a significant difference to the power in the upstream and downstream (Fig. 4.4), and knowing the loading is directly related to the power in the phase-averaged data (Fig. 4.6), we would like to know how does the loading change differently in the upstream and the downstream. Fig. 4.8 and Fig. 4.9 present separate contours for the average coefficient of force ($\overline{C_F}$) and the maximum coefficient of force ($C_{F_{max}}$) for both upstream and downstream conditions. Both plots exhibit similar trends, such as the negative camber airfoil decreases $\overline{C_F}$ and $C_{F_{max}}$ upstream and increases them downstream compared to the symmetric foil when the preset pitch angle is below 0°. Conversely, the positive camber airfoil increases both $\overline{C_F}$ and $C_{F_{max}}$ upstream but decreases them downstream in comparison to the symmetric foil when the preset pitch angle is below 0°. Overall, the effects of the positive camber airfoil on $\overline{C_F}$ and $C_{F_{max}}$ are the exact opposite of the effects of the negative camber, with changes of similar magnitudes in opposite directions and matching regions for operating conditions.

For the symmetric foil, both upstream average loading and maximum loading depend on changes in preset pitch angles and TSR. With additional changes in the geometric camber profile, the upstream loading change is just as dependent on the preset pitch as the symmetric foil and the TSR. In the downstream, both average loading and maximum loading for the symmetric airfoil reach a minimum value when $\alpha_p = -4°$. As the preset pitch angle approaches extreme values, both average and maximum loading diverge from this minimum value. Opting for the minimal loading preset pitch angle downstream would result in an increase in maximum loading upstream, albeit with reduced power compared to the optimal value.

It's noteworthy that the maximum loading upstream has a magnitude of 3.5, while the maximum loading downstream has a magnitude of 1.2. The upstream maximum loading generally has a higher magnitude in regions where the turbine exhibits positive performance. Therefore, when considering maximum loading, the upstream value is crucial. Considering these findings, potential strategies to reduce the maximum loading on the structure include the use of a negative camber airfoil with the optimal preset pitch while having no losses in

power production. Also, the negative camber airfoil operating at a lower preset pitch angle down to -16° could potentially produce power at 50% of the optimal value with a lower maximum value throughout the entire turbine rotation compared to the symmetric airfoil.

Chapter 5
CONCLUSION

The effect of changing the preset pitch angle of cambered airfoils used within cross-flow turbines was experimentally tested and analyzed. Performance was assessed through experimental measurements on a one-bladed turbine, such that contributions to turbine power could be assigned to the blade. This work focuses primarily on the power generation and efficiency of the turbine in combination with the structural loading to open up new opportunities in operating cross-flow turbines with different combinations of preset pitch angle and geometric camber.

The influence of blade rotation on the extent of virtual camber and angle of attack was explored through the conformal mapping method of Migliore et al. by analyzing the equivalent virtual camber and virtual AOA component based on the nominal flow conditions. The virtual camber and virtual AOA have a wider range of fluctuation when at a lower TSR, and the range decreases as the TSR goes up. At TSR = 3.0, the rotationally induced angle of attack, α_r ranges from 4° to 11° with no sensitivity to changing geometric camber as a result of the use of only the chord line in the calculation. The rotationally induced camber, γ_r varies from 4% to 8% as a result of changing preset pitch angles and geometric camber for our turbine. Virtual camber is shown to be more sensitive to changes in the preset pitch angle than changes in the geometric camber. As a result, geometric camber can be experimentally changed without greatly altering the blade dynamics due to rotation.

Overall, a range of TSR from 1.2 to 3.2 in combination with preset pitch angles from $-16°$ to 4° were tested for three airfoils (one symmetric airfoil, and two camber airfoils with $\pm 2\%$ camber at 0.4c). The time-averaged power coefficient near peak performance was seen to be relatively insensitive to preset pitch angle or geometric camber. All three airfoils have

a similar peak performance. Changes in geometric camber have little to no effect on the optimal preset pitch angle for each airfoil. With small variations due to different camber airfoil, the optimal preset pitch angle stays between the range of $-6°$ to $-8°$ due to the limitation from experimental resolution. The negative camber case shows an opportunity to produce power at higher TSRs with an extremely low preset pitch angle at $-16°$. This region is where the symmetrical airfoil shows a negative power coefficient. However, under these conditions, the negative camber airfoil still only produces less than 50% of the power seen under optimal conditions. This operating condition is unlikely to be used.

In general, the maximum phase-averaged performance increases with the tip-speed ratio for the range of tip-speed ratios explored in this study (at higher TSRs it would be expected to reduce at some point). As TSR rises, the phase of peak performance is delayed to later phases of rotation. At low TSR ($\lambda = 1.6$), various preset pitch angles yield similar peak phase-averaged performance, while at higher TSR ($\lambda = 2.4$, $\lambda = 3.0$), increasing preset pitch angle leads to improved peak phase-averaged performance. Notably, the best-performing pitch angle upstream does not align with the best downstream performance. Different camber airfoils exhibit distinct effects: negative camber decreases upstream peak performance but increases downstream, while positive camber has the opposite impact. The study emphasizes the crucial balance between upstream and downstream performance in determining overall turbine performance. The upstream and downstream time-averaged performance shows the turbine power is more sensitive to the change in preset pitch angles at a higher TSR. Changes in performance due to the different geometric camber are more sensitive to the TSR, with little correlation to the preset pitch angle. The performance gain by the camber airfoil from either upstream or downstream is often offset by the performance loss in the other, thus, resulting in no net change in the overall performance in the power-producing region of TSR and preset pitch angle.

The time-averaged in-plane force shows a direct relationship between the turbine performance and the loading. Hence, a better-performing blade experiences a higher average force in most cases. The symmetrical airfoil shows that the coefficient of force remains insensitive

to the preset pitch angle until higher tip-speed ratios are reached, with no change at TSR less than 2.4. At higher TSRs, $\overline{C_F}$ remains constant for preset pitch angles between $-12°$ to $-4°$ and sharply increases at extreme pitch angles. Negative camber generally decreases the average $\overline{C_F}$ across most regions compared to the symmetric foil, except at optimal conditions where it is similar. Positive camber increases the average $\overline{C_F}$ in most regions, especially at higher preset pitch angles. At the optimal combination of TSR and preset pitch angle, all three camber airfoils yield a similar time-averaged coefficient of force, proving that time-averaged force is directly related to time-averaged power.

Similarly, the maximum phase-averaged coefficient of force shows the negative camber airfoil could reduce the maximum structural loading while still producing a similar amount of power. Comparing the maximum load for the negative camber and symmetric foils, there is a decrease in most regions, ranging from -0.3 to -0.7. This is particularly pronounced at the optimal operating point with a -16% change when compared to the symmetric foil. The maximum loading contour distinctly shows a decrease in maximum structural loading for negative camber compared to the symmetric foil. Note the upstream maximum loading is always higher than the maximum loading downstream. In addition, a decrease in the preset pitch angle would reduce the maximum loading upstream but increase the maximum loading downstream. However, with the increased amount of maximum loading downstream, the downstream loading is still lower than the value upstream. This creates an opportunity to reduce the overall maximum loading by sacrificing some performance by operating the turbine with a slightly lower preset pitch angle.

In conclusion, analysis of the rotationally induced virtual blade geometry shows the virtual camber is more dependent on the change in preset pitch angle than the change in geometric camber. Changes in geometric camber impose no effects on the virtual angle of attack. All three camber airfoils show a similar peak time-averaged power production with the same tip-speed ratio. The optimal preset pitch angle is insensitive to the change in the tip-speed ratio or the geometric camber. The time-averaged loading shows a direct relation to power production. Although, the utilization of the 2% camber airfoil does not create a

huge performance gain when compared to the zero camber airfoil when in combination with the preset pitch angle, the negative camber shows a promising reduction in the maximum loading with minimal loss or zero net change in the performance. In addition, operating the turbine at a lower preset pitch angle could also reduce the maximum loading with a small loss in performance.

REFERENCES

[1] Migliore, P. G. and Wolfe, W. P., "Effects of flow curvature on the aerodynamics of Darrieus wind turbines," Tech. rep., West Virginia University, Morgantown, West Virginia, 1980.

[2] Dabiri, J. O., "Potential order-of-magnitude enhancement of wind farm power density via counter-rotating vertical-axis wind turbine arrays," *Journal of renewable and sustainable energy*, Vol. 3, No. 4, 2011.

[3] Migliore, P., Wolfe, W., and Fanucci, J., "Flow curvature effects on Darrieus turbine blade aerodynamics," *Journal of Energy*, Vol. 4, No. 2, 1980, pp. 49–55.

[4] Athair, A., Caelan, C., Han-Wen, C., Jennifer, F., and Williams, O., "Can Cambered Blades Help Cross-Flow Turbine Performance? Part I: Experimental Exploration of Blade Forces and Turbine Performance," In Preparation.

[5] Hunt, A., Strom, B., Talpey, G., Ross, H., Scherl, I., Brunton, S., Wosnik, M., and Polagye, B., "A parametric evaluation of the interplay between geometry and scale on cross-flow turbine performance," *arXiv preprint arXiv:2310.20616*, 2023.

[6] Strom, B., Brunton, S., and Polagye, B., "Consequences of preset pitch angle on cross-flow turbine hydrodynamics," *Proceedings of the 11th European Wave and Tidal Energy Conference*, No. 4, 2015, pp. 08D2–4.

[7] Gregory, P., Joubert, P. N., and Chong, M., *Flow over a body of revolution in a steady turn*, DSTO Platforms Sciences Laboratory, 2004.

[8] Polagye, B., Strom, B., Ross, H., Forbush, D., and Cavagnaro, R. J., "Comparison of cross-flow turbine performance under torque-regulated and speed-regulated control," *Journal of Renewable and Sustainable Energy*, Vol. 11, No. 4, 2019.

[9] Strom, B., Johnson, N., and Polagye, B., "Impact of blade mounting structures on cross-flow turbine performance," *Journal of Renewable and Sustainable Energy*, Vol. 10, No. 3, 2018.

[10] Athair, A., Snortland, A., Scherl, I., Polagye, B., and Williams, O., "Intracycle Control Sensitivity of Cross-Flow Turbines," *Proceedings of the European Wave and Tidal Energy Conference*, Vol. 15, 2023.

[11] Snortland, A., Williams, O., and Polagye, B., "The Influence of the Downstream Blade Sweep on Cross-flow Turbine Performance," *Proceedings of the European Wave and Tidal Energy Conference*, Vol. 15, 2023.

[12] Bianchini, A., Marten, D., Tonini, A., Balduzzi, F., Nayeri, C. N., Ferrara, G., and Paschereit, C. O., "Implementation of the "virtual camber" transformation into the open source software QBlade: validation and assessment," *Energy Procedia*, Vol. 148, 2018, pp. 210–217.

[13] Mandal, A. and Burton, J., "The effects of dynamic stall and flow curvature on the aerodynamics of Darrieus turbines applying the cascade model," *Wind Engineering*, 1994, pp. 267–282.

[14] Migliore, P., Wolfe, W., and Walters, R., "Aerodynamic tests of Darrieus wind turbine blades," *Journal of Energy*, Vol. 7, No. 2, 1983, pp. 101–106.

[15] Akimoto, H., Hara, Y., Kawamura, T., Nakamura, T., and Lee, Y.-S., "A conformal mapping technique to correlate the rotating flow around a wing section of vertical axis wind turbine and an equivalent linear flow around a static wing," *Environmental Research Letters*, Vol. 8, No. 4, 2013, pp. 044040.

[16] van der Horst, S., van de Wiel, J. E., Simao Ferreira, C., and Ramos García, N., "Flow curvature effects for vawt: A review of virtual airfoil transformations and implementation in xfoil," *34th Wind Energy Symposium*, 2016, p. 1734.

[17] Balduzzi, F., Bianchini, A., Maleci, R., Ferrara, G., and Ferrari, L., "Blade design criteria to compensate the flow curvature effects in H-Darrieus wind turbines," *Journal of Turbomachinery*, Vol. 137, No. 1, 2015, pp. 011006.

[18] Strom, B., Polagye, B., and Brunton, S., "Hydrodynamic Optimization of Cross-Flow Turbines with Large Chord to Radius Ratios," *Proc. 3rd Mar. Energy Technol. Symp., Washington, DC*, 2015.

[19] Bhutta, M. M. A., Hayat, N., Farooq, A. U., Ali, Z., Jamil, S. R., and Hussain, Z., "Vertical axis wind turbine–A review of various configurations and design techniques," *Renewable and Sustainable Energy Reviews*, Vol. 16, No. 4, 2012, pp. 1926–1939.

[20] Ross, H. and Polagye, B., "An experimental assessment of analytical blockage corrections for turbines," *Renewable Energy*, Vol. 152, 2020, pp. 1328–1341.

[21] Hunt, A., Stringer, C., and Polagye, B., "Effect of aspect ratio on cross-flow turbine performance," *Journal of Renewable and Sustainable Energy*, Vol. 12, No. 5, 2020.